aPKCλ controls epidermal homeostasis and stem cell fate through regulation of division orientation

Michaela T. Niessen,[1,2] Jeanie Scott,[1] Julia G. Zielinski,[1] Susanne Vorhagen,[1] Panagiota A. Sotiropoulou,[3] Cédric Blanpain,[3] Michael Leitges,[4] and Carien M. Niessen[1]

[1]Department of Dermatology, Center for Molecular Medicine Cologne, Cologne Excellence Cluster on Cellular Stress Responses in Aging-Associated Diseases (CECAD), University of Cologne, 50931 Cologne, Germany
[2]International Graduate School for Genetics and Functional Genomics (IGS-GFG), University of Cologne, 50674 Cologne, Germany
[3]Interdisciplinary Research Institute (IRIBHM), Université Libre de Bruxelles (ULB), 1070 Brussels, Belgium
[4]Biotechnology Centre of Oslo, University of Oslo, N-0317 Oslo, Norway

The atypical protein kinase C (aPKC) is a key regulator of polarity and cell fate in lower organisms. However, whether mammalian aPKCs control stem cells and fate in vivo is not known. Here we show that loss of aPKCλ in a self-renewing epithelium, the epidermis, disturbed tissue homeostasis, differentiation, and stem cell dynamics, causing progressive changes in this tissue. This was accompanied by a gradual loss of quiescent hair follicle bulge stem cells and a temporary increase in proliferating progenitors. Lineage tracing analysis showed that loss of aPKCλ altered the fate of lower bulge/hair germ stem cells. This ultimately led to loss of proliferative potential, stem cell exhaustion, alopecia, and premature aging. Inactivation of aPKCλ produced more asymmetric divisions in different compartments, including the bulge. Thus, aPKCλ is crucial for homeostasis of self-renewing stratifying epithelia, and for the regulation of cell fate, differentiation, and maintenance of epidermal bulge stem cells likely through its role in balancing symmetric and asymmetric division.

Introduction

Regulation of cell fate is not only essential in development but also for tissue homeostasis. To maintain the different tissue lineages that arise from adult stem/progenitor cells, tissues have to balance self-renewal with differentiation. Stem/progenitor cells can achieve this dual act through oriented cell division, a process regulated by polarity proteins. Whereas symmetric cell division (SCD) generates two daughters with similar fate, asymmetric cell division (ACD) produces daughter cells with differential fates. In lower organisms, it is well established that ACD promotes tissue differentiation, which is essential during development and for tissue homeostasis (Knoblich, 2010; Goulas et al., 2012).

An open question is whether ACD is also used to maintain homeostasis in self-renewing adult mammalian epithelial tissues. For example, conflicting reports exist if intestinal epithelial stem cells use ACD to couple self-renewal to differentiation (Quyn et al., 2010; Snippert et al., 2010; de Navascués et al., 2012; Goulas et al., 2012), while lineage tracing experiments in the epidermis suggest an important role for ACD in the maintenance of the interfollicular epidermis (Clayton et al., 2007; Mascré et al., 2012; Poulson and Lechler, 2012).

The mouse epidermis is a self-renewing stratifying epithelium consisting of the interfollicular epidermis (IFE) and its appendages, the sebaceous glands and hair follicles (HFs). The maintenance of these different epidermal lineages is driven by different populations of stem and progenitor cells, each of which is characterized by one or more markers (Blanpain and Fuchs, 2009; Watt and Jensen, 2009). The IFE, the sebaceous gland, and the permanent part of the HF undergo life-long self-renewal, whereas the nonpermanent part of the HF undergoes cycles of growth (anagen), regression (catagen), and rest (telogen). Thus, the epidermis provides an excellent model system to address the role of ACD and its regulators in tissue homeostasis, differentiation, and cell fate determination.

During development of the epidermis, the plane of cell cleavage rotates in basally dividing cells concurrent with the

The Rockefeller University Press $30.00
J. Cell Biol. Vol. 202 No. 6 887–900
www.jcb.org/cgi/doi/10.1083/jcb.201307001

JCB **887**

onset of stratification. This results in apical–basal divisions (asymmetric) as opposed to basal–basal (symmetric) divisions (Smart, 1970; Lechler and Fuchs, 2005). The basal daughter remains positive for the basal cell marker keratin 14, the now suprabasally positioned daughter turns on keratin 10, a suprabasal marker (Poulson and Lechler, 2010). Conversely, interfering with the molecular machinery shown to regulate spindle positioning in asymmetrically dividing *Drosophila* neuroblasts shifted the balance toward symmetric cell division (SCD) in the developing epidermis and reduced stratification (Williams et al., 2011). These results indicate that in the developing IFE, ACD produces progeny with different cell fates and promotes differentiation. Together, these observations link key regulators of spindle positioning to differentiation in mammalian epithelial cells.

In lower organisms the polarity protein atypical protein kinase C (aPKC) controls cell fate and ACD by coupling the orientation of the mitotic spindle to the polarized segregation of cell fate determinants (Lee et al., 2006; Knoblich, 2010), resulting in two daughter cells with differential fate. Whether aPKCs determine division orientation and cell fate in mammals is less clear. Mammals contain two genes encoding aPKCs: aPKCζ and aPKCλ/ι (in mouse aPKCλ). Whole-body inactivation of aPKCλ results in early embryonic lethality (Soloff et al., 2004), whereas aPKCζ knockouts are viable with no obvious skin phenotype (Leitges et al., 2001). This is in line with findings that aPKCλ is more ubiquitously expressed in embryos compared with aPKCζ (Kovac et al., 2007). Whereas in vitro and ex vivo studies indicate an important role for aPKCλ and/or aPKCζ in spindle orientation and cell fate (Dard et al., 2009; Hao et al., 2010; Durgan et al., 2011), in vivo inactivation in the hematopoietic or neuronal systems indicate no essential role for aPKCs in these processes (Imai et al., 2006; Sengupta et al., 2011).

Here we assessed the role of atypical PKC in a self-renewing epithelium by inactivating aPKCλ in the interfollicular epidermis and its appendages. These results show that aPKCλ is crucial for epidermal homeostasis, regulation of differentiation, and maintenance of epidermal bulge stem cells likely through its role in balancing symmetric and asymmetric division in different compartments of the epidermis.

Results

In the newborn epidermis aPKCλ is expressed in all epidermal layers with enrichment at intercellular junctions in suprabasal layers, whereas aPKCζ localizes predominantly to the cytoplasm and nucleus in the basal layer (Helfrich et al., 2007). Real-time PCR analysis showed a much higher expression for aPKCλ than for aPKCζ in newborn (40-fold) and adult (10-fold; Fig. S1 A) mice, which was further confirmed by Western blot analysis (Fig. S1 D). Thus, aPKCλ is the predominant aPKC expressed in mouse epidermis.

To ask whether aPKC regulates polarity and cell fate in the epidermis, we therefore inactivated aPKCλ specifically in all layers of the epidermis and its appendages. To this end, aPKCλ floxed mice (Farese et al., 2007) were crossed to mice expressing the Cre-recombinase under the control of the K14 promoter (Hafner et al., 2004). This resulted in efficient deletion

of aPKCλ in all layers of the IFE and its appendages, as shown by real-time PCR, Western blot, and immunofluorescence analysis (Fig. S1, B–E). Deletion of aPKCλ induced a slight increase in aPKCζ RNA expression (Fig. S1 C).

Inactivation of aPKCλ did not result in any obvious macroscopic and histological changes in newborn mice (Fig. 1, A and B). However, starting at postnatal day 6 (P6) aPKCλ[epi−/−] mice developed an increasingly pronounced hair phenotype (Fig. 1 A), characterized by different extents of hair loss in individual mice followed by hair regrowth. Histologically, this was accompanied by a gradual increase in IFE thickness (Fig. 1, B and C), an expansion of the upper areas of the HF, the so-called junctional zone (JZ) and infundibulum, increasingly enlarged sebaceous glands, and increasing numbers of irregularly shaped HFs (Fig. 1 B and Fig. S2 A and B).

Most strikingly, whereas at P20 all control HFs were in the first resting (telogen) phase of the HF cycle, around 60% of aPKCλ^{−/−} follicles were showing signs of anagen, the growth stage of the HF cycle (Fig. 1 B). To examine if this was due to a slower or faster cycling or, alternatively, due to a failure to properly transit into the next phase, we characterized a range of postnatal days that cover the different stages of the first and second cycle (Fig. 1 E), as these are synchronous in mice. At P16 only around 40% of aPKCλ^{−/−} HFs compared with control were in catagen, the retraction phase of the HF cycle, and a similar percentage were transiting into the telogen resting phase at P18, already indicating disturbed cycling upon loss of aPKCλ (Fig. S2 A). Both control and aPKCλ^{−/−} HFs were in anagen at P33. Whereas controls went into second catagen at P42 and subsequently telogen (P49 and P58), all aPKCλ^{−/−} HFs remained in an anagen-like state at all later stages tested, even though there were morphological signs of catagen induction at P42 and P49 around the dermal papilla. This resulted in significantly longer HFs at P58 in aPKCλ[epi−/−] mice when control HFs were in telogen (Fig. 1 D). These data indicate that aPKCλ^{−/−} HFs are continuously in anagen and fail to properly undergo phases of retraction and rest (Fig. 1 B; Fig. S2). Thus, epidermal-specific inactivation of aPKCλ results in gradual morphological changes in different lineages of the epidermis.

Altered differentiation in the epidermal lineages

To examine if the observed morphological alterations in the IFE, sebaceous gland, and HF are accompanied by changes in differentiation we stained for a range of differentiation markers. Loricrin, a late IFE differentiation marker, showed increased staining in the aPKCλ-deficient IFE (Fig. 2 A). Staining for SCD1, a marker for mature sebocytes (Miyazaki et al., 2001), also revealed an increased number of differentiated sebaceous gland cells in aPKCλ[epi−/−] mice, compared with control mice (Fig. 2 B). These sebocytes were functional, as they secreted lipids as indicated by increased Nile red staining (Fig. 2 C). Thus, loss of aPKCλ alters the differentiation of the IFE and promotes sebaceous gland differentiation.

To ask whether epidermal loss of aPKCλ interfered with HF differentiation, we examined the expression and localization of several keratins (K) that mark the different layers of the
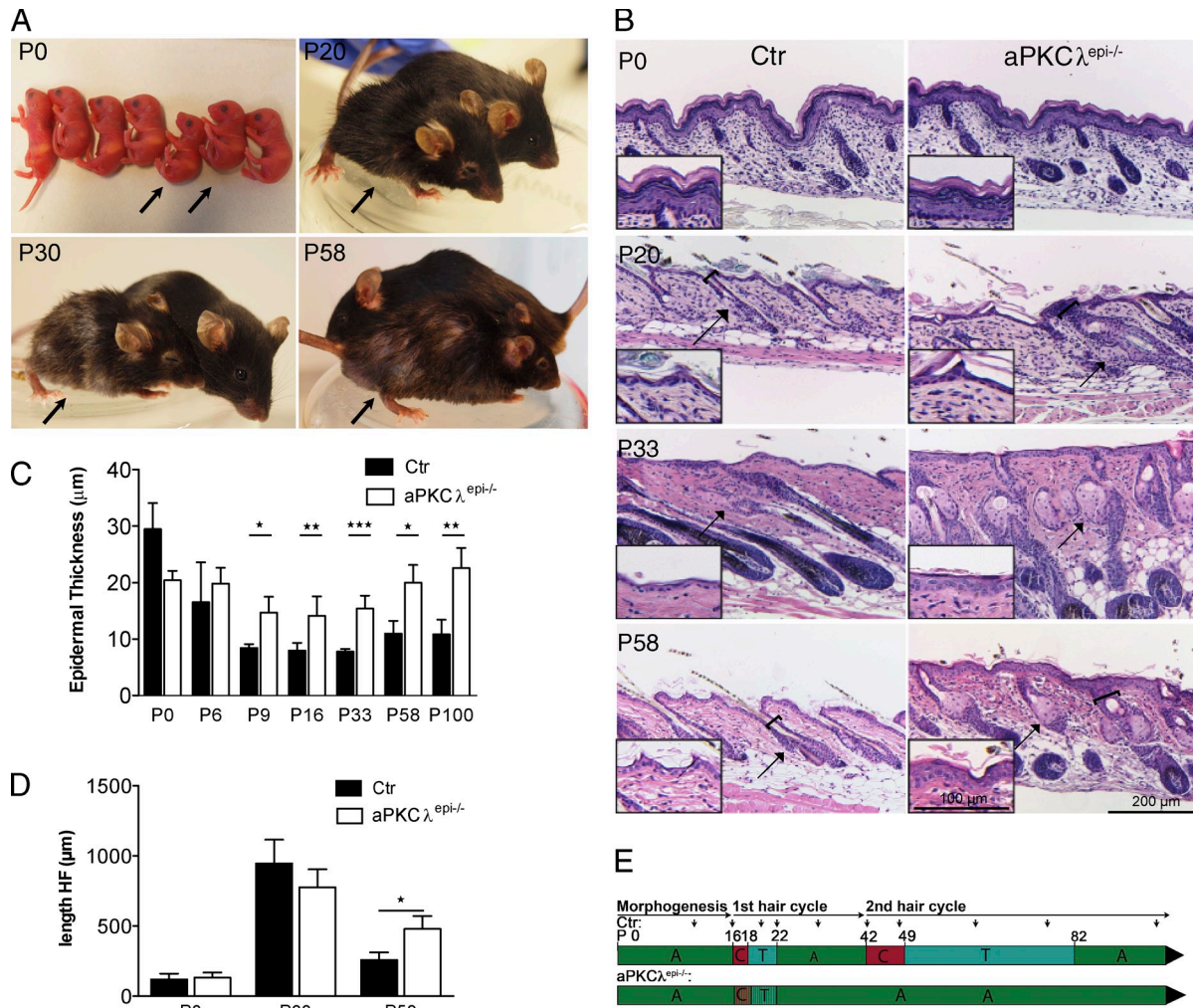
Figure 1. **Epidermal loss of aPKCλ results in cyclic hair loss and altered hair follicle cycling.** (A) Macroscopic appearance of control (Ctr) and aPKCλ[epi−/−] (black arrows) littermates at different postnatal (P) days. (B) Gradually developing epidermal phenotype of aPKCλ[epi−/−] mice. Hematoxylin and Eosin (H&E) staining of paraffin sections of back skin from Ctr and aPKCλ[epi−/−] mice at the indicated postnatal days. Black arrows indicate increased SGs and black brackets indicate increased width of the infundibulum. (C) Quantification of epidermal thickness (without stratum corneum) using H&E stained sections of back skin from Ctr and aPKCλ[epi−/−] mice at indicated postnatal days. $n > 4$ mice/genotype. Data are presented as mean ± SD. *, $P < 0.05$; **, $P < 0.01$; ***, $P < 0.001$. (D) Quantification of hair follicle (HF) length in skin from Ctr and aPKCλ[epi−/−] mice from the indicated postnatal (P) days. $n = 4$ mice/genotype. Data are presented as mean ± SD. *, $P < 0.05$. (E) Schematic representation of hair cycle stages at indicated postnatal time points (P) in Ctr vs. aPKCλ[epi−/−] mice. Anagen (A), green; catagen (C), red; telogen (T), turquoise. HF cycle time is based upon C57/BL6 mice.

HF (Langbein et al., 2004). Global gene expression analysis (Fig. S3 A) and real-time PCR analysis revealed a significantly reduced expression of several hair keratins (Fig. 2 D) marking the inner root sheath (IRS, K28), the cuticle (K35, K82, K85), the cortex (K35, K81, K85), medulla (K28, K6, K75), or companion layer (K75, K6; Schweizer et al., 2007). In agreement, staining for K82 was almost absent in the aPKCλ[epi−/−] mice, whereas staining for K75 and K81 was reduced (Fig. 2 E). In addition, keratin 6 (K6), which also marks a recently identified population of CD34^{−/−} cells located in the bulge (Hsu et al., 2011) revealed a slightly reduced staining in the lower aPKCλ^{−/−} HF whereas it showed an extended localization toward the JZ in aPKCλ^{−/−} HFs (Fig. 2 F). Western blot analysis further confirmed reduced protein expression of K75 and K82 (Fig. S3 B). Ultrastructurally, hairs in aPKCλ[epi−/−] mice had lost their regular pattern (Fig. 2 G), indicating that the observed changes in

differentiation in the HF results in the formation of aberrant hair. Together, these data show that aPKCλ is essential for proper differentiation within the HF lineage of the epidermis.

Increased proliferation and loss of quiescence of bulge stem cells

We next addressed whether the continuous anagen state induced by loss of aPKCλ and the increased width of the junctional zone and infundibulum was driven by increased proliferation. Whereas short term BrdU incorporation was comparable in newborn mice, an increased number of BrdU-positive cells were seen in the IFE (see Fig. 7 A) and all compartments of aPKCλ^{−/−} HFs compared with control, including the infundibulum/JZ and the bulge compartment (Fig. 3, A and B; see Fig. 7, B and C). This suggested that the hair follicle stem cells (HFSCs) located in the bulge have lost quiescence. Real-time PCR analysis
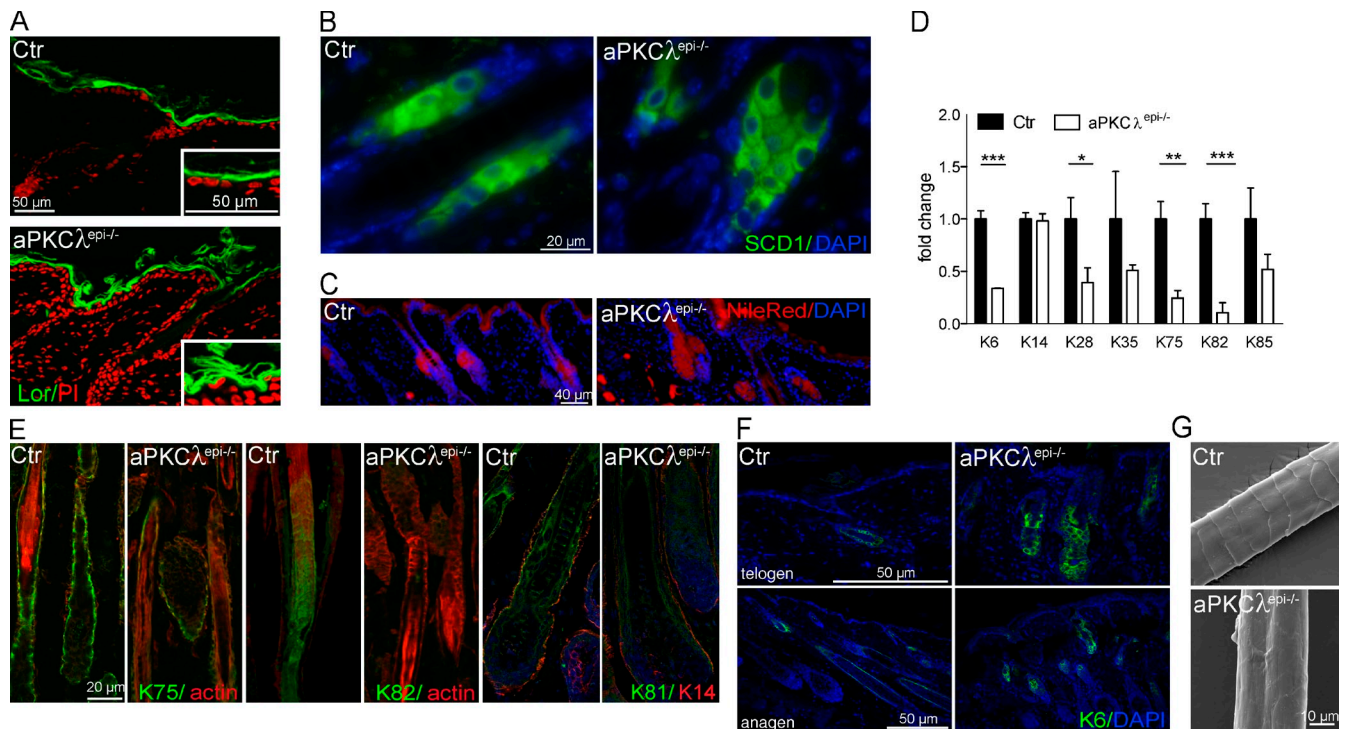
Figure 2. **Altered differentiation in different epidermal lineages upon loss of aPKCλ.** (A) Loricrin staining (green) on skin sections of P58 mice. Nuclei were counterstained with propidium iodide (PI, red). (B and C) Sebaceous gland differentiation. (B) Immunohistochemical staining for SCD1 (green) and (C) staining for Nile red (red) on cryo-preserved dorsal skin sections of Ctr and aPKCλ$^{epi-/-}$ mice (P6 and P9). Nuclei were counterstained with DAPI. (D–G) Analysis of hair follicle differentiation. (D) Real-time RT-PCR analysis of indicated keratins (K) on RNA isolated from P33 epidermis of Ctr and aPKCλ$^{epi-/-}$ mice. (E) Immunohistochemical analysis of K75 or K82 (green) and actin (red) or K81 (green), K14 (red), and DAPI (blue) on P33 back skin cryo-preserved sections of Ctr and aPKCλ$^{epi-/-}$ mice. (F) Immunohistochemical analysis of K6 (green) on P18 (top) and P33 (bottom) paraffin back skin sections. Nuclei were counterstained with DAPI. (G) Scanning electron microscopy analysis of hair from of adult (P60) aPKCλ$^{epi-/-}$ mice and Ctr littermates showed altered hair morphology and structure in aPKCλ-deficient mice.

showed an increase in aPKCλ but not aPKCζ expression in CD34-positive bulge stem cells compared with CD34-negative non-bulge cells (Fig. S4 A), suggesting a specific role for aPKCλ in this population. BrdU label-retaining experiments revealed a loss of label retention in K15-positive bulge stem cells (Fig. 3, C and D) and a loss of nuclear localization of NfatC1 (Fig. 3 E), a marker for quiescence. These results indicate a specific role for aPKCλ in the regulation of HFSC quiescence in the bulge.

Gradual loss of bulge stem cells

We next examined whether the increase in proliferation and loss of quiescence of bulge HFSC in aPKCλ$^{-/-}$ HFs reflected a more activated bulge stem population (Zhang et al., 2006; Kobielak et al., 2007; Horsley et al., 2008) or was accompanied by alterations in bulge stem cell identity (Castilho et al., 2009; Yang et al., 2009). Staining for the bulge stem cell marker CD34 revealed a strongly reduced signal in P58 aPKCλ$^{-/-}$ HFs compared with control (Fig. 4 A). Quantitative FACS analysis showed no statistically significant difference at P33 in the number of integrin α6/CD34 double-positive cells, whereas a successive decline in numbers was observed in increasingly older aPKCλ$^{epi-/-}$ mice (Fig. 4 B), indicating a gradual depletion of bulge HFSCs. In agreement, no obvious difference in the bulge stem cell markers S1006A or K15 was observed at P33 (Fig. S4, B and C), whereas these markers were reduced in P58 mice (Fig. 4 C; Fig. S4 C). Sox9, a marker that is enriched in bulge

HFSCs (Blanpain et al., 2004; Morris et al., 2004), was no longer confined to the bulge (Fig. S4 D). Apoptosis was increased in all epidermal compartments at P33 (not depicted), including in K15-positive bulge HFSCs (Fig. 4 D). Although this might contribute to the loss of HFSCs, it is likely counterbalanced by the more pronounced increase in proliferation (Fig. 3 B). Thus, inactivation of aPKCλ results in a gradual loss of bulge stem cells.

Increase in proliferating junctional zone progenitors

We next asked whether the gradual decrease in bulge HFSCs was accompanied by a concomitant increase in more committed, proliferative progenitors, as was suggested by the expansion of the isthmus region and JZ of aPKCλ$^{-/-}$ hair follicles. We therefore examined expression of Lrig1, a marker that labels a recently identified progenitor population located in the JZ, which mainly fuels the IFE and the sebaceous glands (Jensen et al., 2009). MTS24 is a marker that recognizes a highly clonogenic population in the isthmus/JZ (Nijhof et al., 2006). Immunofluorescence analysis revealed an increase in the area positive for Lrig1 and MTS24 (Fig. 5, A and B). Co-staining with K15 revealed no obvious overlap between K15 and MTS24 (Fig. S5 A). As bulge K6 (Hsu et al., 2011) staining expanded more toward the JZ (Fig. 2 F) in aPKCλ$^{-/-}$ HF, we also examined the overlap between K15 and K6 and found a slightly reduced overlap of these
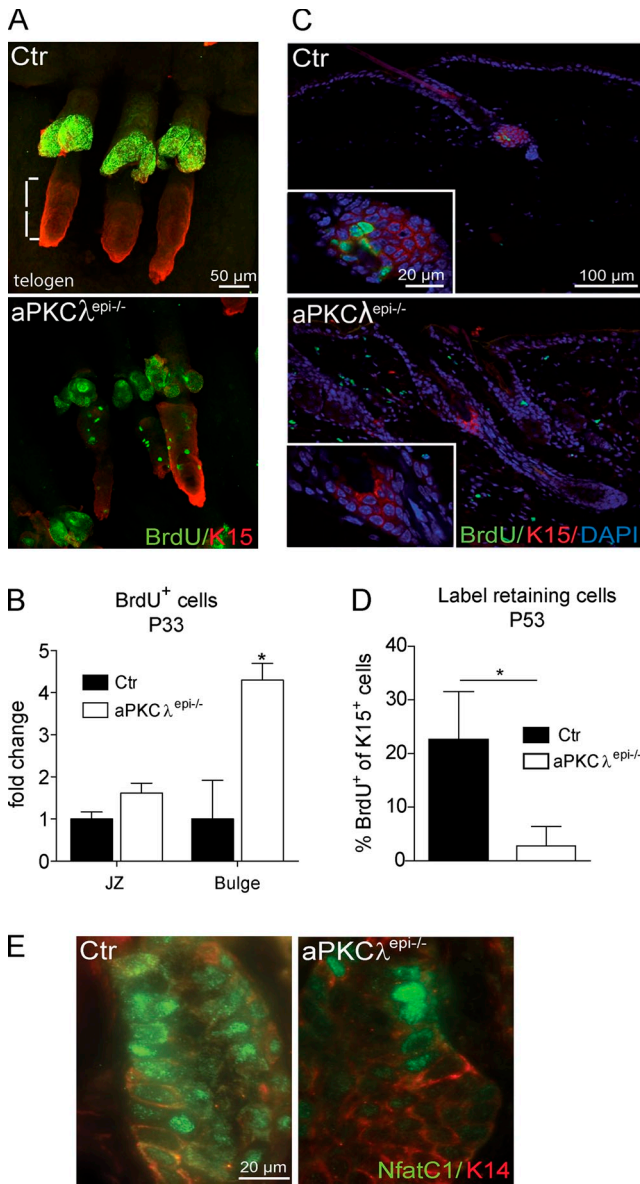
Figure 3. **Increased proliferation and loss of quiescence in the bulge.** (A) Whole-mount immunofluorescence analysis of BrdU (green) and K15 (red) of P18 tail skin of control and aPKCλ$^{epi-/-}$ mice. White brackets mark HF bulge region in the control. (B) Quantification of BrdU-positive cells of back skin sections in the HF bulge region and junctional zone (JZ) of P30 mice. Mice were injected with BrdU and sacrificed after 30 min. $n > 4$ mice/genotype. Data are presented as mean ± SD. *, $P < 0.05$. (C) Immunofluorescence analysis of BrdU in tail epidermis of control and aPKCλ$^{epi-/-}$ mice at P53, 41 d after BrdU injections. Bulge cells were counterstained with K15 and nuclei with DAPI. (D) Quantification BrdU label–retaining bulge cells from C. $n = 3$ mice/genotype. Data are presented as mean ± SD. *, $P < 0.05$. (E) Immunofluorescence analysis for NfatC1 and K14 on paraffin sections of p58 dorsal skin.

markers in aPKCλ$^{-/-}$ HFs compared with control. (Fig. S5 A) FACS analysis showed a gradual increase in the number of cells positive for either MTS24 (Fig. 5 C) or Lrig1 (Fig. S5 B) when comparing P33 to P58 mice. Taken together, epidermal inactivation of aPKCλ results in an accumulative phenotype characterized by a gradual decrease in quiescent epidermal bulge stem cells accompanied by an increase in the number of proliferative more committed progenitor cell populations. This increase in

proliferative progenitors may drive HFs into a continuous anagen-like state while also expanding the JZ, infundibulum, and sebaceous glands.

Cell fate changes upon loss of aPKCλ in Lrg5-positive HF stem cells

To examine whether loss of aPKCλ would alter the cell fate of bulge HFSCs toward more committed progenitors, thus explaining the increase in more committed progenitors, we crossed aPKCλ$^{fl/fl}$ mice with Lgr5Cre^{ERT2}eGFP mice (Barker et al., 2007) and with Rosa26R-LacZ Cre-reporter mice (Soriano, 1999). Tamoxifen administration to Lgr5-Cre^{ERT2};aPKC$^{fl/fl}$;Rosa26R-LacZ mice resulted in deletion of aPKCλ (Fig. S5 C) and expression of β-galactosidase in a considerable number of Lgr5 progeny (Fig. 5, D–F). At P21, when HFs are in telogen, Lgr5 is exclusively expressed in the lower bulge and hair germ HFSCs and its progeny contribute to the lower part of the hair follicle but not to the JZ, infundibulum, and IFE (Jaks et al., 2008). Upon tamoxifen-induced activation of Cre at P21, control Lgr5 progeny were labeled by β-galactosidase and contributed exclusively to the lower nonpermanent part of control hair follicles (Fig. 5, D and E). In contrast, aPKCλ$^{-/-}$/β-galactosidase–positive Lrg5 progeny were not only found in the lower HF, but also in JZ, infundibulum, and IFE (Fig. 5, D and E). Occasionally, β-galactosidase–positive cells could be observed in the sebaceous glands (Fig. 5 F, top right inset). Most importantly, aPKCλ$^{-/-}$/β-galactosidase–positive cells in the JZ expressed the JZ marker Lrig1 (Fig. 5 F) and aPKCλ$^{-/-}$ JZ cells no longer expressed K15 although they are stem cell descendants (Fig. 5 G), whereas K15$^+$/aPKC$^{-/-}$ cells could be found in the bulge (Fig. 5 G, inset). Together, these data show that upon loss of aPKCλ, Lgr5-positive bulge stem cells contribute to the JZ and IFE. Thus, aPKCλ directs cell fate changes coupled to the regulation of proliferation in the epidermal lineage.

Loss of aPKCλ promotes asymmetric divisions in the IFE and HF

In lower organisms aPKC regulates asymmetric divisions to couple spindle orientation to cell fate determination and differentiation (Knoblich, 2010). Several recent papers demonstrated an important role for ACDs in promoting stratification during interfollicular epidermal morphogenesis (Poulson and Lechler, 2010; Williams et al., 2011). Immunofluorescence analysis showed that aPKCλ localized asymmetrically in the apical domain both in asymmetric and symmetric divisions (Fig. 6 A), as has been reported previously (Lechler and Fuchs, 2005).

We next addressed whether aPKCλ regulates asymmetric versus symmetric divisions in the epidermis and thereby determines cell fate and differentiation. SCD and ACD were scored as described previously (Williams et al., 2011) using the spindle midbody marker survivin (Fig. 6 B). As ACD versus SCD are best characterized in the developing IFE we first assessed how loss of aPKCλ alters the ratio in these divisions (Fig. 6, C and D). At E16.5 61% of divisions were scored as asymmetric, 7% as random, and 31% as symmetric in control. Loss of aPKCλ did not result in a significant increase in random spindle orientation (10%) in the developing epidermis, as might have been
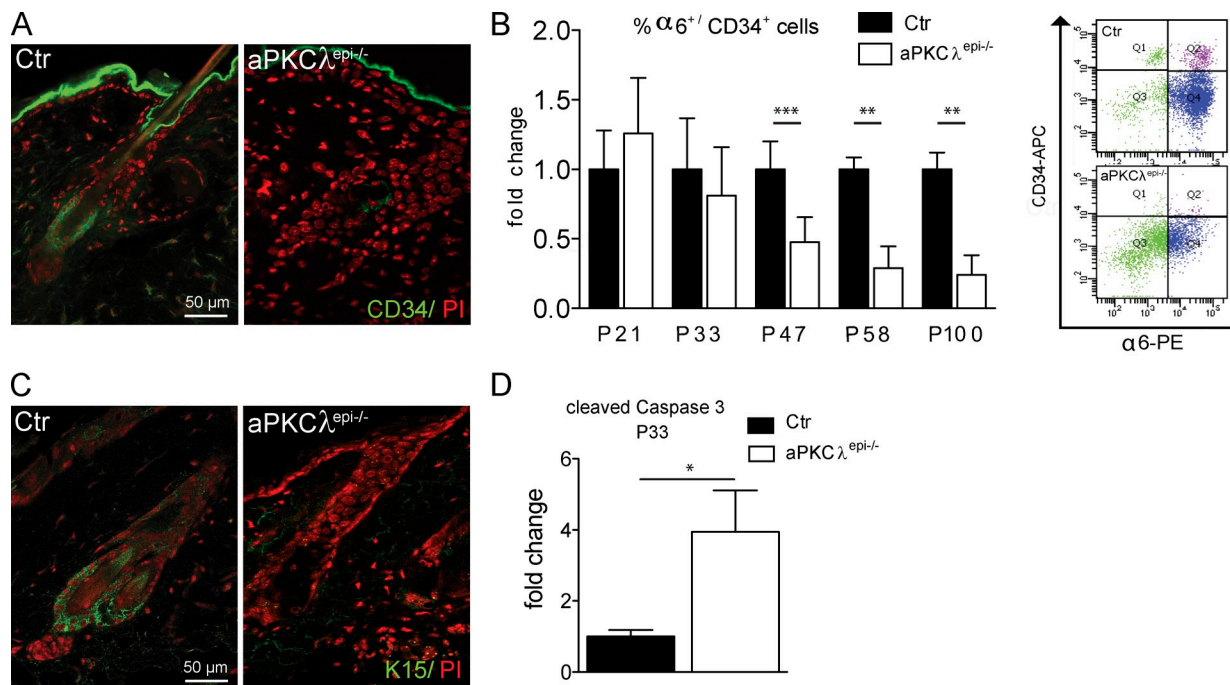
Figure 4. Gradual loss of bulge hair follicle stem cells (HFSCs). (A) Immunohistochemical analysis of CD34 on paraffin sections of P58 Ctr and aPKCλ$^{epi-/-}$ back skin. Nuclei were counterstained with propidium iodide (PI). (B) Quantification (left) of FACS analysis (right, P58) of integrin α6$^+$/CD34$^+$ bulge HFSCs from epidermis at indicated time points revealed a gradual loss of bulge HFSCs. The percentage of α6$^+$/CD34$^+$ cells from control animals was set at 1. $n =$ 5 mice/genotype. Data are presented as mean ± SD. *, $P < 0.05$; **, $P < 0.01$; ***, $P < 0.0001$. (C) Immunofluorescence analysis of K15 on paraffin sections of P58 Ctr and aPKCλ$^{epi-/-}$ back skin. Nuclei were counterstained with propidium iodide (PI). (D) Quantification of cleaved caspase 3–positive cells in K15$^+$ bulge stem cell compartment on back skin sections of P33 Ctr and aPKCλ$^{epi-/-}$ mice. $n = 3$ mice/genotype. Data are presented as mean ± SD. *, $P < 0.05$.

predicted on the basis aPKC function in ACDs in *Drosophila* and *Caenorhabditis elegans* (Knoblich, 2010). Instead, a shift of around 20% from SCD (10%) to ACD (80%) was observed in the IFE of E16.5 aPKCλ$^{epi-/-}$ mice (Fig. 6, C and D). A similar increase in ACDs was also observed in the adult IFE (Fig. 6, E and F), indicating that aPKCλ also regulates the orientation of division during homeostasis of the IFE. Most importantly, loss of aPKCλ shifted spindle orientation toward more asymmetric in HFs at all stages examined, as judged by angles of division in relation to the long axis of HF growth (Fig. 6, G and H). This shift was not only observed in the hair matrix (not depicted), but also in the JZ, the physical localization of Lrig/MTS24-positive cells, and, importantly, also in the bulge stem cell compartment (Fig. 6, I and J). Thus, loss of aPKCλ results in a consistent shift of around 20–30% toward ACDs in different regions within the epidermis and its appendages, thereby providing a mechanism for the gradual alterations in cell fate and differentiation observed in these epidermal lineages.

We next examined if aPKCλ determines the localization of other proteins implicated in the regulation of SCD and ACD. No obvious difference was observed in the localization of the aPKC-binding partner Par3 or the cell fate determinant Numb or NuMA (Fig. 6 K). As loss of aPKCλ did not increase random spindle orientations, these results are perhaps not so surprising. More importantly, these findings suggest that the mechanisms by which aPKCλ regulates asymmetric divisions are different from those in *Drosophila* and *C. elegans*, and identify a novel role for aPKCλ in balancing asymmetric and symmetric divisions that may determine cell fate in the epidermal lineage.

Temporary increase of proliferation and loss of proliferative potential

The observed shift of around 20% toward more ACDs induced by loss of aPKCλ is consistent with the gradually developing phenotype in aPKCλ$^{epi-/-}$ mice and with the observed loss of quiescent bulge stem cells. As more ACDs were also observed in the JZ, the region where the Lrig1+ and MTS24+ cells reside, one would predict that the increase in proliferation in these cells is temporary, as these committed progenitors have less proliferative potential. Short-term BrdU incorporation assays revealed that whereas proliferation was initially increased in the IFE (Fig. 7 A), the HF (Fig. 7 B), and JZ (Fig. 7 C), this increase was indeed temporary, as no significant difference in proliferation was observed in older mice either in the IFE (Fig. 7 A) in the HF (Fig. 7 B), and more specifically in the JZ (Fig. 7 C). This temporary increase in proliferation could be recapitulated in vitro, as aPKCλ$^{-/-}$ keratinocytes isolated from newborn mice grew faster and showed increased proliferation compared with newborn control keratinocytes (Fig. 7 E). In contrast, adult aPKCλ$^{-/-}$ keratinocytes showed a highly differentiated appearance (Fig. 7 D), were strongly inhibited in growth, and incorporated less BrdU (Fig. 7 E). To examine whether the gradual stem cell marker loss was reflected by a loss of HFSC function, indicating a loss of HFSCs, we performed colony formation assays to examine proliferative potential (Barrandon and Green, 1987; Morris and Potten, 1994). Whereas keratinocytes isolated from newborn aPKCλ$^{epi-/-}$ mice showed a similar proliferative potential as newborn control keratinocytes, aPKCλ$^{-/-}$ keratinocytes isolated from adult mice were strongly impaired in their
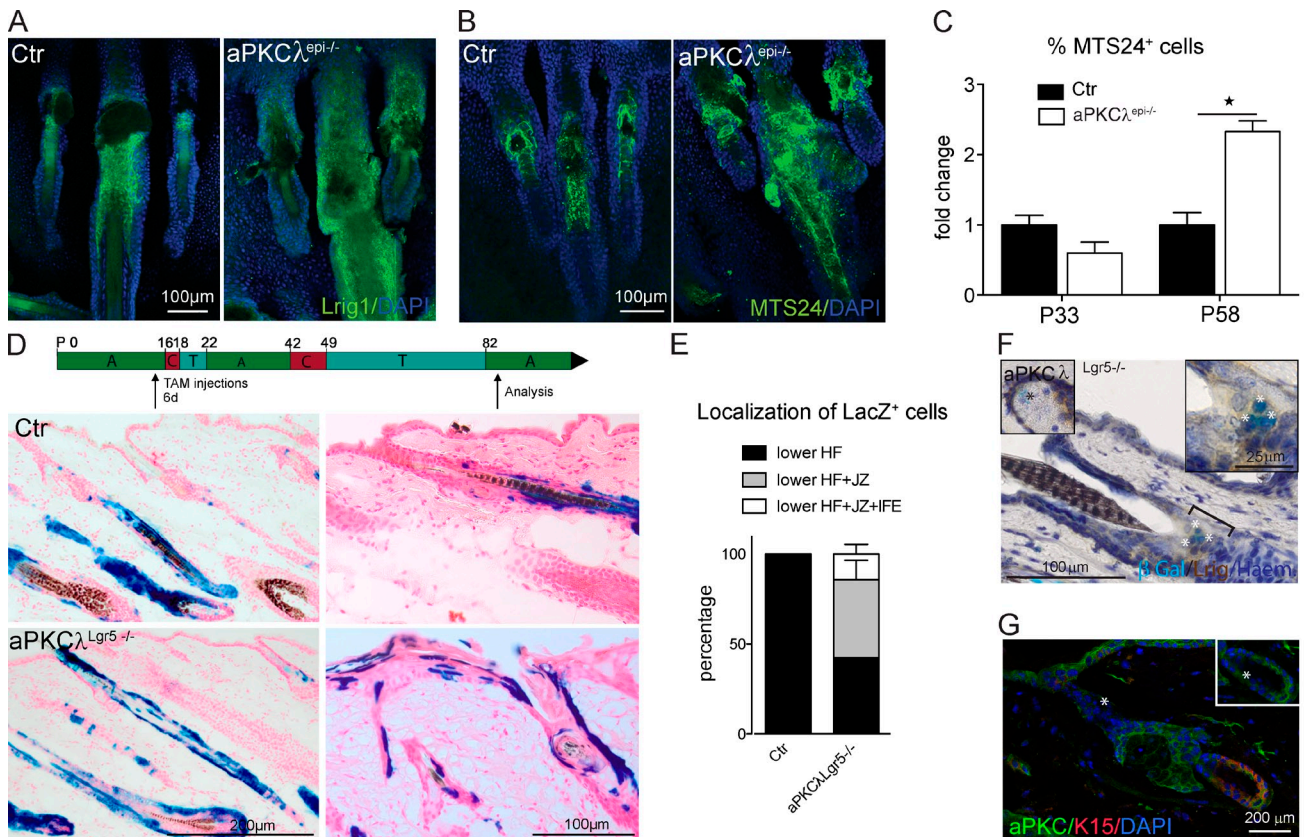
Figure 5. **Loss of aPKCλ results in increase in junctional zone progenitors and cell fate changes of bulge stem cells.** (A and B) Immunofluorescence analysis of Lrig1 (A) or MTS24 (B) on P33 whole mounts of Ctr and aPKCλ[epi−/−] tail skin. Nuclei were counterstained with DAPI. (C) FACS analysis quantification of MTS24+ keratinocytes from P33 and P58 epidermis. The percentage of MTS24+ cells in control was set as 1. $n = 3$ mice/genotype for each time point. Data are presented as mean ± SD. *, $P < 0.05$. (D) Lineage-tracing analysis of β-galactosidase–positive Lgr5 progeny from Ctr and aPKCλ[lgr5−/−] mice. Animals were injected at P21 for six consecutive days with 1 mg tamoxifen and analyzed at P85. Cryo-preserved dorsal skin sections were stained for β-galactosidase and nuclei counterstained with nuclear red. (E) Quantification of percentage of hair follicles with different localization of lineage-traced Lrg5 progeny grouped into: "Lower HF": hair follicles with LacZ+ cells only in the region between dermal papilla and junctional zone; "lower HF + JZ": HF with LacZ+ cells in lower HF and in the junctional zone (JZ) between SGs and IFE; "lower HF + JZ + IFE": HF with LacZ+ cells in lower HF, the JZ, and IFE. $n = 4$ mice/genotype. Data are presented as mean + SD. (F) Co-stainings of junctional zone marker Lrig1 (brown) and β-galactosidase (turquoise, white asterisk) on cryo-preserved back sections of P85 aPKCλ[lgr5−/−] mice. Nuclei were stained with haemalaun (blue). Top left inset: same magnification, shows a LacZ+ sebaceous gland cell (black asterisk). Top right inset: higher magnification of Lrig+/LacZ+ cells. (G) Immunofluorescence analysis of aPKC and K15 on paraffin sections of P85 aPKCλ[lgr5−/−] mice to show that JZ aPKCλ^{−/−} cells do not express K15. Inset: aPKC staining only of K15-labeled bulge to show aPKCλ^{−/−} cells, same magnification.

colony-forming ability, indicating a gradual loss of proliferative potential and thus of stem cell function, indicative of loss of HFSCs (Fig. 7 F).

Premature aging in aPKCλ[epi−/−] mice

If epidermal loss of aPKCλ induces a depletion of bulge stem cells over time, this should ultimately result in a loss of the lower HF compartment and baldness in older mice. One-year-old aPKCλ[epi−/−] mice indeed almost completely lost their hair coat and, more importantly, do not regain their hair, indicating alopecia in these mice (Fig. 8 A). Morphological analysis revealed a loss of the lower HF compartment in aPKCλ^{−/−} HFs, which in these mice predominantly consists of mature sebaceous glands (Fig. 8 B), as further shown by staining for the SC marker SCD1 and the lipid stain Nile red (Fig. 8 C). FACS analysis for MTS24+ JZ progenitor cells revealed that the increase initially observed was temporary (Fig. 8 E), whereas the area positive for Lrig1 was still expanded compared with control (Fig. S5 D). Melanocytes were scattered in the dermis (Fig. 8 B, inset), in line with the observation that aPKCλ[epi−/−] mice show premature greying of hairs before they lose their hair coat

(not depicted). This also indirectly indicated a loss of the melanocyte stem cell niche, which is constituted by the bulge HFSCs (Tanimura et al., 2011). Indeed, no positive staining could be observed for the bulge stem cell marker CD34 in immunofluorescence (Fig. S5 E) in aPKCλ^{−/−} HFs, which was further confirmed by FACS analysis (Fig. 8 D), indicating a complete loss of bulge stem cells in these mice.

Discussion

The balance between self-renewal and differentiation of adult stem and progenitor cells drives tissue homeostasis. In the present manuscript we identify a crucial role for the polarity protein aPKCλ in balancing self-renewal of epidermal stem/progenitor cell populations with differentiation to control epidermal homeostasis. Epidermal loss of aPKCλ disturbed homeostasis, as reflected in an increase in the number of differentiated SG cells, altered IFE differentiation, a continuous anagen-like HF state, and disturbed HF differentiation. In addition, loss of aPKCλ resulted in an activation and gradual loss of quiescent epidermal
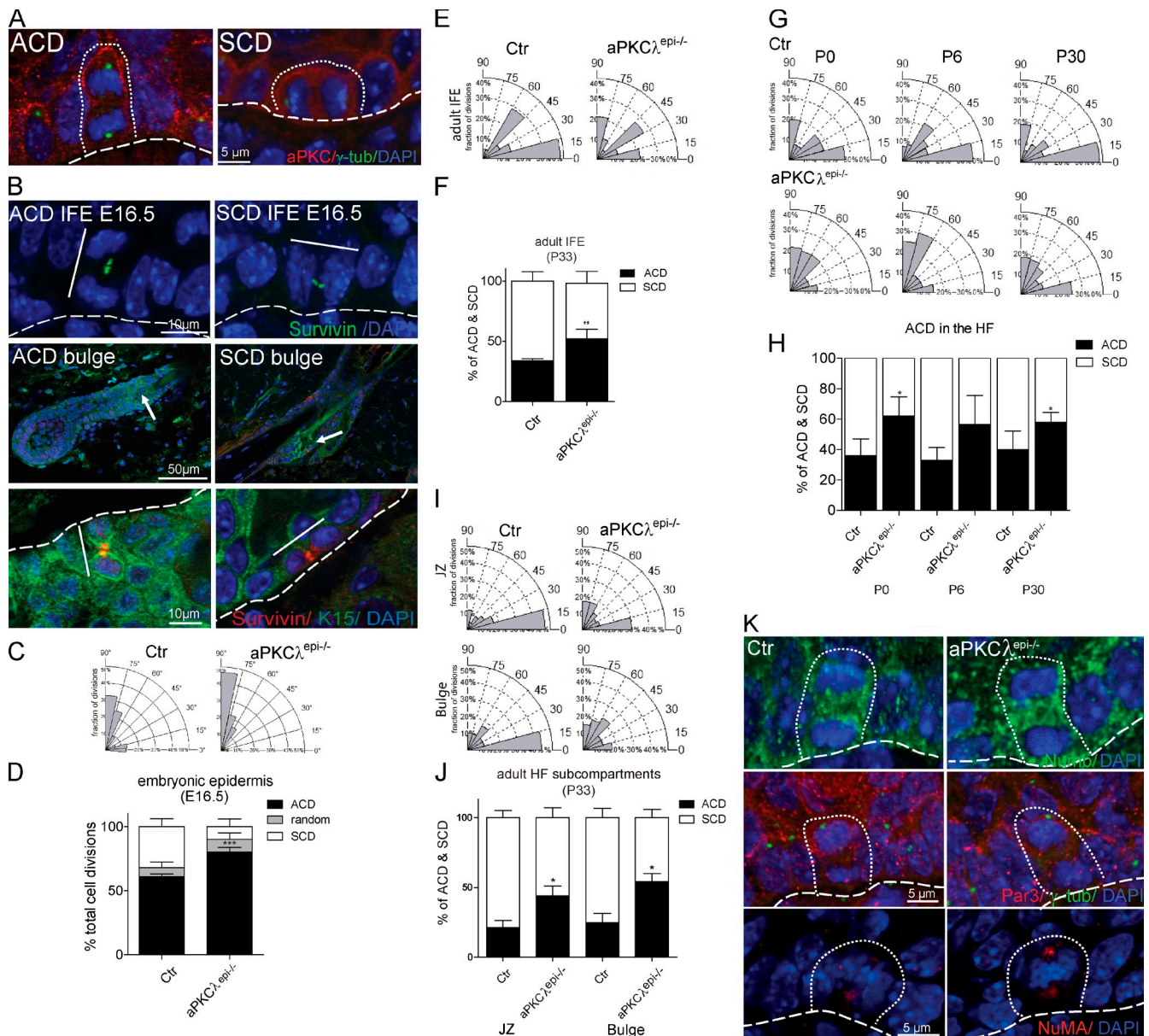
Figure 6. **Shift toward asymmetric cell divisions upon loss of aPKCλ in interfollicular epidermis and hair follicles.** (A) aPKCλ is localized apically in asymmetrically and symmetrically dividing cells in E16.5 control epidermis. Co-staining with γ-tubulin to mark centrosomes. Nuclei were counterstained with DAPI. (B) Co-staining of Survivin and DAPI to visualize asymmetrically and symmetrically dividing cells in the basal layer of the IFE at E16.5 and hair follicle bulge regions at P33. Co-staining with K15 to mark the bulge region. ACD: asymmetric cell division scored as perpendicular to basement membrane (E16.5) or long HF growth axis (Bulge, broken lines). SCD: symmetric cell division, in parallel to basement membrane (E16.5) or long hair follicle growth axis. (C) Radial histogram quantification of division angles in E16.5 IFE. (D) Percentage of asymmetric (ACD; 60–90°C), symmetric (SCD; 0–30°C), or random (30–60°) divisions in E16.5 basal layer. $n = 5$ mice/genotype with $n = 145$ and $n = 158$ divisions analyzed from control and aPKCλ[epi−/−] mice. Data are presented in mean values ± SD. ***, P < 0.0001. (E) Radial histogram quantification of division angles in P33 IFE. (F) Percentage of ACD and SCD in the IFE basal layer of P33 mice. 78 and 112 divisions analyzed from $n = 4$ of control and aPKCλ[epi−/−] mice. Data are presented as mean values ± SD. **, P < 0.01. (G) Radial histogram quantification of division angles in HFs at different ages. (H) Percentage of ACD and SCD in hair follicles at several postnatal days. More than 25 divisions were analyzed at P0: $n = 6$ Ctr and $n = 5$ aPKCλ[epi−/−] mice; P6: $n = 4$ Ctr and $n = 2$ aPKCλ[epi−/−] mice; and P30: $n = 6$ Ctr and $n = 5$ aPKCλ[epi−/−] mice. Data are presented as mean values ± SD. *, P < 0.05. (I) Radial histogram quantification of division angles in bulge and junctional zone of P33 mice. (J) Percentage of ACD and SCD in different HF subcompartments at P30–P33 from Ctr and aPKCλ[epi−/−] mice. JZ, junctional zone: 34 (Ctr) and 58 (aPKCλ[epi−/−]) divisions; Bulge: 29 (Ctr) and 38 (aPKCλ[epi−/−]) divisions from $n > 5$ different mice. Data are represented in mean values ± SD. *, P < 0.05. (K) Immunofluorescent staining of Numb, Par3, and NuMA in the basal layer of control and aPKCλ^{−/−} epidermis at E16.5. Nuclei were counterstained with DAPI and centrosomes were visualized with γ-tubulin staining (Par3). Broken line marks basement membrane, dotted line surrounds dividing cells.

bulge stem cells while initially expanding more committed proliferating progenitors. Lineage tracing revealed that the increase in more committed progenitors descend from bulge cells. Subsequently, these cells are also gradually lost in older mice,

ultimately leading to premature hair loss. Together, these findings indicate a role for aPKCλ in the regulation of epidermal stem cells, differentiation, and cell fate. This is accompanied by a shift of around 20% toward more ACDs in all epidermal
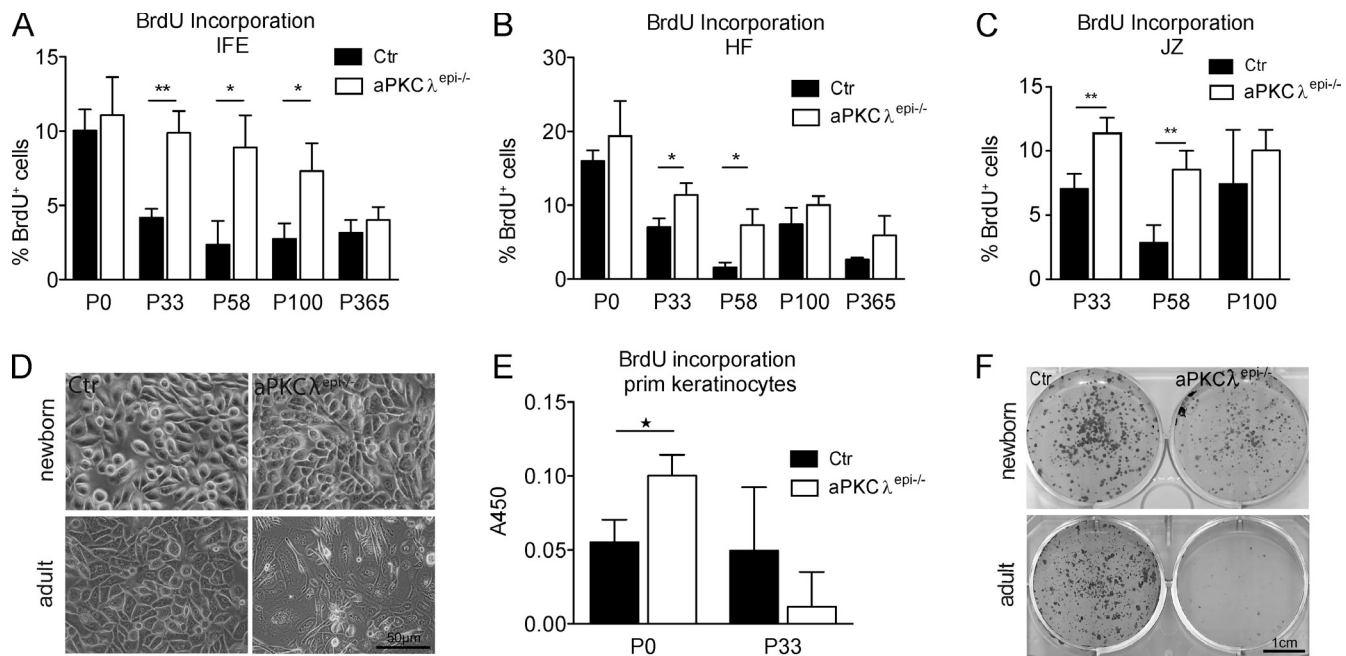
Figure 7. **Transient increase of in vivo and in vitro proliferation accompanied by loss of proliferative potential.** (A–C) Quantification of BrdU-positive cells in (A) the IFE, (B) the HF, and (C) the JZ from back skin sections of control and aPKCλ$^{epi-/-}$ mice at the indicated postnatal days. $n > 3$ mice/genotype. Data are presented as mean ± SD. *, $P < 0.05$; **, $P < 0.01$. BrdU was injected 30 min before the mice were scarified. (D) Phase-contrast micrographs of primary Ctr and aPKCλ$^{-/-}$ keratinocytes isolated from either newborn (P0) or adult (P33) aPKCλ$^{epi-/-}$ and Ctr mice. (E) Brdu incorporation assay showing increased proliferation of primary aPKCλ$^{-/-}$ keratinocytes isolated from newborn and decreased proliferation of aPKCλ$^{-/-}$ keratinocytes isolated from adult mice (P33) compared with control. Proliferation was determined using a colorimetric BrdU incorporation assay. $n = 3$ independently isolated cell cultures/genotype. Data are presented as mean ± SD. *, $P < 0.05$. (F) Representative example of a colony-forming assay using primary keratinocytes from newborn (P0) or adult (P33) Ctr and aPKCλ$^{epi-/-}$ mice show a strongly reduced proliferative potential in primary aPKCλ$^{-/-}$ keratinocytes isolated from adult but not newborn mice. $n = 7$ independently isolated cell cultures/genotype.

compartments examined. Asymmetric divisions promote differential daughter cell fate (Knoblich, 2010) and have been shown to drive in vivo differentiation and age-dependent depletion of neuronal stem cells (Encinas et al., 2011). These data would thus predict that the observed shift toward ACD induced by loss of aPKCλ would drive inappropriate differentiation and stem cell exhausting, as is indeed observed. We thus propose that balancing the ratio of ACDs versus SCDs is the cellular mechanism by which aPKCλ regulates epidermal cell fate, stem cell behavior, differentiation, and epidermal homeostasis.

Loss of aPKCλ inhibits carcinogenesis in different mouse models, whereas overexpression of aPKCλ is observed in a range of human cancer (Fields et al., 2007). Our findings provide a potential explanation for how increased aPKCλ might drive carcinogenesis. By promoting symmetric divisions aPKCλ would drive expansion of a more undifferentiated stem cell–like population. In line with our data, aPKCλ is indeed essential for K-Ras–dependent expansion of bronchioalveolar stem cells in a mouse lung cancer model (Regala et al., 2009).

Although aPKCs couple oriented divisions to cell fate in lower organisms (Rolls et al., 2003; Lee et al., 2006; Baye and Link, 2007; Sabherwal et al., 2009; Goulas et al., 2012), this is not clear in mammals. Several in vitro studies identified a role for aPKCs in the regulation of mammalian division orientation (Hao et al., 2010; Durgan et al., 2011). In contrast, neither aPKCλ nor aPKCζ is essential for in vivo mammalian neuronal differentiation (Leitges et al., 2001; Imai et al., 2006), a process regulated by the balance between ACD and SCD (Miyata et al.,

2010). Intestinal loss of aPKCλ also does not obviously interfere with intestinal architecture and homeostasis (Murray et al., 2009), indicating that aPKCλ is expendable for intestinal stem cell differentiation. However, the presence of the other isoform might compensate for loss of aPKCλ function in these organs. More importantly, inactivation of both isoforms did not affect hematopoietic stem cell polarization and hematopoiesis under steady-state and stressed conditions (Sengupta et al., 2011), indicating that aPKCs are dispensable in this tissue. As our data show that aPKCλ controls the ACD/SCD balance in the epidermis, these results suggest that mammalian tissues have differential requirements for aPKCs in the regulation of oriented cell division coupled to cell fate decisions and differentiation.

The mechanisms by which aPKCλ regulates the balance between symmetric and asymmetric divisions are less clear. Whereas loss of aPKCs resulted in random spindle orientation in *C. elegans* or in vitro (Dard et al., 2009; St Johnston and Ahringer, 2010; Durgan et al., 2011), in vivo epidermal loss of aPKCλ caused a shift toward more ACDs. In contrast, in vivo knockdown of known regulators of spindle orientation, such as NuMa or Lgn, promote SCDs in the developing interfollicular epidermis (Williams et al., 2011). This suggests that aPKCλ does not directly interfere with the machinery crucial for spindle orientation. In agreement, the localization of NuMa was also not obviously altered in asymmetrically dividing aPKCλ$^{-/-}$ keratinocytes at E16.5 (Fig. 6). Moreover, although total protein levels of the cell fate determinant Numb were reduced (not depicted), localization was not altered (Fig. 6 K). Inducible
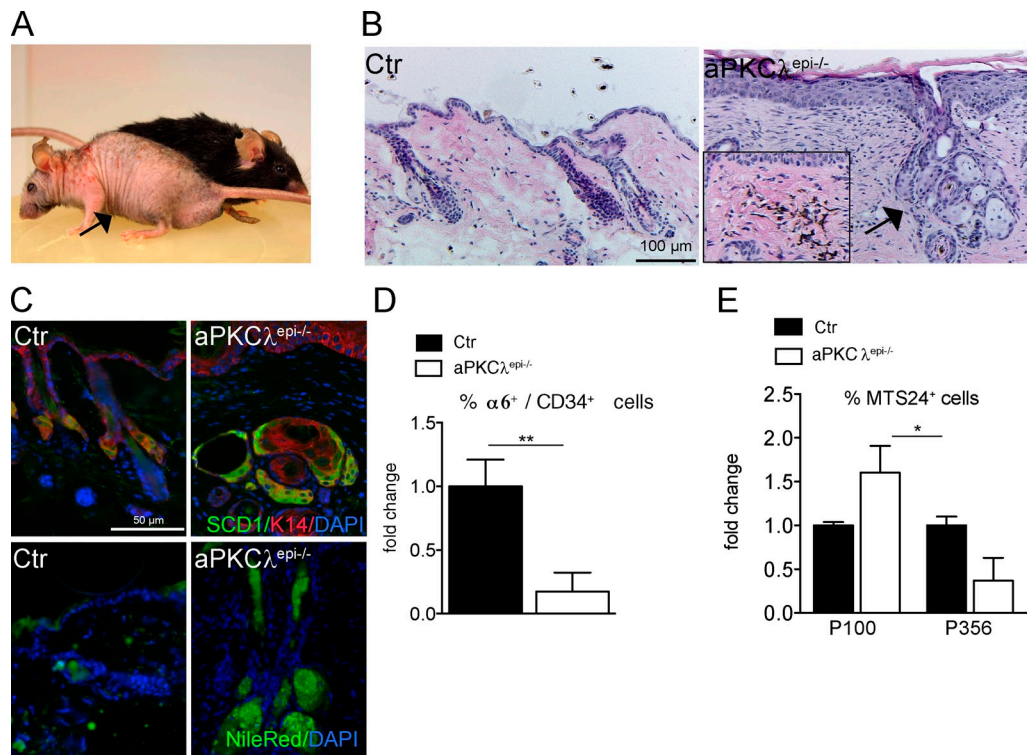
Figure 8. **Loss of aPKCλ induces premature aging of the skin.** (A) Macroscopic appearance of one-year old (P365) aPKCλ$^{epi-/-}$ mice (black arrow) and control littermates. (B) H&E staining of paraffin sections of P365 back skin from Ctr and aPKCλ$^{epi-/-}$ mice. Inset: scattering of melanocytes in dermis, same magnification. (C) Increased SG differentiation in one-year-old aPKCλ$^{epi-/-}$ mice. Immunohistochemical staining for SCD1, K14, and DAPI (top) or Nile red staining and DAPI (bottom) on P365 back skin sections. (D) Quantification of FACS analysis of integrin α6$^+$/CD34$^+$ bulge hair follicle stem cells isolated from P365 mice. The percentage of α6$^+$/CD34$^+$ control cells from was set at 1. $n = 4$ mice/genotype. Data are presented as mean ± SD. **, $P < 0.01$. (E) Quantification of FACS analysis of MTS24$^+$ cells isolated from control (set at 1) and aPKCλ$^{epi-/-}$ mice at indicated postnatal days. n = at least 3 mice/genotype. Data are presented as mean ± SD. **, $P < 0.01$.

epidermal overexpression of Inscutable (Insc), the adaptor protein that couples aPKC to NuMA and Lgn in *Drosophila* neuroblasts, initially promotes ACDs, but in contrast to loss of aPKCλ, this effect is reversed upon prolonged Insc expression and accompanied by dissociation of NuMA (Poulson and Lechler, 2010). These results suggest that aPKCλ does not balance ACDs/SCDs through Insc. Moreover, mice with an epidermal loss of the aPKC binding partner Par3 reach adulthood apparently normally and deletion of Par3 was not reported to disturb skin homeostasis (Iden et al., 2012). As keratinocytes still express aPKCζ, albeit in low amounts, this might be sufficient to drive spindle orientation in the absence of aPKCλ. Together, the data identify aPKCλ as essential for balancing ACD/SCD and suggest that aPKCλ may either actively inhibit ACDs or promote SCDs in the epidermis.

Interestingly, loss of aPKCλ did not only shift the balance toward ACD in developing and adult IFE but also in different compartments of the HF, including the hair bulge stem cell compartments. A previous report showed that whereas HFSCs divide predominantly symmetrically, hair germ cells divide asymmetrically in late telogen and at the onset of anagen (Zhang et al., 2009). The shift toward more asymmetric divisions in the aPKCλ$^{-/-}$ HF bulge was accompanied by activation and a gradual loss of bulge stem cells as reflected by a loss of quiescence, increased proliferation, and loss of bulge stem cell markers and proliferative potential. In addition, aPKCλ$^{-/-}$ HFs were in

continuous anagen accompanied by an expansion of JZ and infundibulum and increased thickening of the IFE. Lineage tracing showed that aPKCλ$^{-/-}$ but not control lower bulge cells contribute to these regions. Thus, the increase in ACD observed upon loss of aPKCλ may cause bulge stem cells to differentiate not only toward hair bulb progenitors to provide sufficient cells for the continuous anagen-like state, but also may fuel at least in part the expanded upper HF region of aPKCλ$^{-/-}$ HFs.

We did observe an increase in apoptosis not only in the HFSCs but also in other compartments of the epidermis. However, this was counterbalanced by an increase in proliferation. As we did not observe an obvious overlap between more differentiated markers K6, MTS24 (Fig. S5 A), or SCD1 (not depicted) and the bulge HFSC marker K15, it is unlikely that loss of aPKCλ drives intrinsic premature HFSC differentiation. The increase in ACD is one of the earliest changes observed (E16.5) upon loss of aPKCλ and precedes changes in proliferation and apoptosis. Together, the data suggest that the loss of HFSCs is not the result of increased apoptosis or intrinsic premature differentiation, but instead is driven by the shift toward more ACD that may drive inappropriate cell fate changes in the bulge.

Although our initial data show no obvious change in migration in aPKCλ$^{-/-}$ keratinocytes (unpublished data), we can at present not rule out that inappropriate migration and disturbed homing of bulge stem cells (Hsu et al., 2011) also contribute to the anagen-like HF state or the expansion of the infundibulum

and the IFE. How loss of aPKCλ affects the in vivo dynamics of ACD/SCDs and migratory behavior in the hair follicle bulge, hair germ, and infundibulum will be an important subject for further studies. Nevertheless, our data clearly demonstrate that aPKCλ is required to maintain the bulge HFSC compartment throughout postnatal life.

The loss of bulge stem cells was accompanied by an increase in Lrig1^{+} and MTS24^{+} progenitor cells. As loss of aPKCλ also promoted ACD in the JZ this would predict that this increase would be temporary. For MTS24^{+} cells, that was indeed what we observed in older mice. However, the Lrig1-positive area was still expanded in the one-year-old mice (unpublished data), thus supporting the notion that MTS24^{+} and Lrig1^{+} cells represent different progenitor populations (Jaks et al., 2010). As lineage tracing has shown that descendent of bulge stem cells progress first into the MTS24^{+} region followed by progression into the Lrig1^{+} compartment (Petersson et al., 2011), this would suggest that cells either end in the Lrig1^{+}-positive population or are depleted even later. Nevertheless, despite the increased expression of Lrig[+] progenitors in vivo, aPKCλ^{−/−} keratinocytes ultimately are no longer hyperproliferative in vivo and have lost their ability to proliferate and form large colonies in vitro. This confirms the in vivo observation of a loss of stemness over time. In older mice the loss of stemness is reflected by the loss of hair, scattered melanocytes, and degenerated HFs that mostly consist of differentiated sebaceous glands. Thus, we observe that an increase in ACD is accompanied by a depletion of stem cells and premature alopecia. A similar observation was recently made in the adult hippocampus, where asymmetric divisions contribute to the age-related depletion of neural stem cells (Encinas et al., 2011). In conclusion, our data identify a key role for aPKCλ in the maintenance of stem cells and epidermal homeostasis and in the regulation of cell division orientation coupled to differentiation.

Materials and methods

Generation of mice with an (inducible) epidermal deletion of aPKCλ
aPKCλ^{fl/fl} mice were generated by insertion of loxP sites flanking nucleotides 110–233 (exon 2) of the published aPKCλ cDNA (Bandyopadhyay et al., 2004; Farese et al., 2007). To achieve epidermis-specific deletion of aPKCλ, female aPKCλ^{fl/fl} mice were crossed to male K14-Cre; aPKCλ^{fl/+} mice (Hafner et al., 2004). Heterozygous inactivation of aPKCλ did not result in any obvious phenotype. As controls either K14-Cre; aPKC^{fl/+}, aPKCλ^{fl/+}, or aPKCλ^{fl/fl} mice were used. The aPKCλ^{fl/fl} mice were backcrossed for six generations to a C57BL/6 background and experiments were performed according to institutional guidelines and animal license of the State Office North Rhine-Westphalia, Germany. To achieve inducible deletion of aPKCλ and simultaneous expression of β-galactosidase in bulge/hair germ stem cells for lineage trace experiments aPKCλ^{fl/fl} mice were crossed with Lgr5-EGFP-Ires-CreERT2 mice (Barker et al., 2007) and Rosa26R-Lacz Cre reporter mice. Cre recombinase was activated in Lgr5-EGFP-Ires-CreERT2; aPKCλ^{fl/fl}/Rosa26-LacZ mice by injecting 10 mg tamoxifen dissolved in 50 μl sunflower oil at six consecutive days. As controls Lgr5-EGFP-Ires-CreERT2; aPKCλ^{fl/+} or aPKCλ^{+/+}/Rosa26-LacZ mice were used. Mice were analyzed in the second anagen at P85.

Genotyping of mice
Tail biopsies were taken from 3-wk-old mice and incubated in lysis buffer (0.2 M NaCl; 0.1 M Tris/HCl, pH 8.5, 5 μm EDTA, 0.2% SDS, and 100 μg/ml proteinase K) for 4 h at 55°C and 500 rpm. DNA was extracted using a standard DNA-isolation protocol with phenol-chloroform and precipitated with isopropanol. Genotyping was performed with customized primers (aPKCλ:

wt, 5′-TTGTGAAAGCGACTGGATTG-3′; aPKCλ355bp, 5′-AATTGTTCAT-GTTCAACACTGCT-3′; aPKCλdel, 5′-ACTAAGCATTGCCTGGCATC-3′; aPKCλ1kb, 5′-CTTGGGTGGAGAGGCTATTC-3′; K14: K14-2202snew: 5′-GATGAAAGCCAAGGGGAATG-3′; CreSL2as, 5′-CATCACTCGTTGCA-TCGACC-3′).

Epidermal splits
Epidermis was separated from the dermis after floating skin biopsies, epidermal side up, in 0.5 M ammonium thiocyanate (NH$_4$SCN) in phosphate buffer, pH 6.8 (0.1 M Na$_2$HPO$_4$ and 0.1 M KH$_2$PO$_4$) for 20 min on ice (Tunggal et al., 2005). Epidermis was either snap-frozen in liquid nitrogen or immediately processed for RNA isolation or protein lysates.

Western blot analysis
Epidermal splits were homogenized in lysis buffer (1% NP-40, 0.5% deoxycholate and 0.2% SDS, 150 mM NaCl, 2 mM EDTA, 0.8 mM EGTA, 10 mM Tris-HCl, pH 7.4, and Complete protease inhibitors [1:25; Roche]) using PreCellys (Peqlab). Equal amounts of protein were separated by SDS-PAGE (Invitrogen), transferred to PVDF membranes, and incubated with the appropriate primary and secondary antibodies. Antibody binding was visualized by ECL. For antibodies used and dilutions see Table S1.

Histology
Mice were collected and dissected at several embryonic and postnatal days. For short-term proliferation analysis, 50 mg/kg BrdU (Sigma Aldrich) was injected for 0.5–1 h before sacrificing mice. Back (dorsal) skin was either snap-frozen in TRIzol (Invitrogen) for subsequent RNA isolation, embedded in optimal cutting temperature (OCT) compound (Tissue-Tek) for cryo sections or fixed in 4% PFA for 12 h for paraffin sections. After fixation in 4% PFA, samples were perfused with xylene followed by paraffin to enable paraffin embedding. Cryo or paraffin sections were sectioned for immunohistochemistry (4–8 μm) and dried on glass coverslips for histological staining.

Isolation and staining of tail skin whole-mounts
Tail epidermis was separated from the dermis after incubation for 3 h at 37°C in 5 mM EDTA/PBS and fixed in 4% formal saline or 0.2% glutaraldehyde for 2 h at room temperature (Braun et al., 2003). Epidermal sheets were blocked for 1 h in TBS buffer (20 mM Hepes, pH 7.2, and 0.9% NaCl) containing 0.5% milk powder, 0.25% fish gelatin, and 0.5% Triton X-100. After incubation with primary antibodies over night at room temperature, whole-mounts were washed in PBS/0.2% Tween 20 for 4 h. Secondary antibodies were then applied over night at room temperature and washing steps were repeated for 4 h. The stained whole mounts were mounted in gelvatol and stored at 4°C.

Immunohistochemistry and β-galactosidase assay
Paraffin sections were deparaffinized and antigens were retrieved with buffer A, UG, or AG (Murray et al., 2009). Freshly cut cryo-sections were fixed in ice-cold acetone and blocked in PBS containing 5% normal goat serum and 0.1% Triton X-100. Slides were incubated with primary antibody in blocking buffer followed by incubation with the appropriate secondary antibodies coupled to Alexa Fluor 488, Alexa Fluor 594, or Cy3 (Invitrogen) and nuclei counterstained with propidium iodide or DAPI (Sigma-Aldrich). For co-staining with β-galactosidase Lrig1 staining was performed on cryo-sections with an HRP-coupled goat antibody (R&D Systems) overnight at 4°C. HRP detection was performed with liquid DAB + substrate chromogen system (Dako) followed by the β-galactosidase assay. 6-μm cryo-sections were fixed in 0.2% glutaraldehyde for 10 min at room temperature. Samples were washed 3 times for 5 min in rinse buffer (2 mM MgCl$_2$ and 0.1% Nonidet P40 in PBS) and stained for 36–48 h in a solution consisting of 1 mg/ml X-gal, 5 mM K$_3$Fe(CN)$_6$, and 5 mM K$_4$Fe(CN)$_6$ in rinse buffer.

Microscopy
Images were taken at room temperature using the fluorochromes DAPI, Alexa Fluor 488 (green), and Alexa Fluor 594 (red). For antibodies used and dilutions see Table S1. Confocal images were taken with an Olympus BX-81 microscope (software: Olympus FluoView FV1000; objectives: 20×/0.85 oil; 40×/1.3 oil; 60×/1.35 oil) or Zeiss Meta LSM 510 microscope (software: Zen 2009; objectives: 10×/0.3; 20×/0.5; 40×1.3 oil; 63×/1.4 oil). Fluorescence images were taken with an Olympus Delta-Vision IX-71 microscope (camera: CoolSnap HQ2; software: Applied Precision Softworx; deconvolution: nearest neighbor; magnifications: 20×/0.75; 10×/0.40; 40×/1.35 oil; 60×/1.42 oil). Bright-field microscopy was

performed using a Leica DM4000B microscope (software: Diskus V4.5; magnifications: 5×/0.15; 10×/0.40; 10×) or Olympus BX-51 microscope (camera: Olympus XC-50; software: Olympus Cell D; objectives: 10×/0.4; 20×/0.75; 40×/0.4). Cell culture and mouse images were taken using an Olympus E-620 camera (lens: Zuiko Digital ED 14–42 mm 1:3.5–5.6). Scanning electron microscopy was done on a JSM-5910 microscope (JEOL). For further image processing, Adobe Photoshop CS5.1/CS2 and Illustrator CS5.1/CS4 were used. Table S2 contains a list of which microscope was used in the different figures.

Isolation of primary newborn and adult keratinocytes
Newborn mice were sacrificed by decapitation and sterilized by incubation for 1 min in iodine solution, sterile PBS, and 70% EtOH. Skin was removed from the torso and floated, dermal side down, on 1 ml of cold 0.25% trypsin solution (without EDTA; Gibco). After incubation for 15–24 h at 4°C epidermis was separated from the dermis, minced with scalpels, and transferred into 1.5 ml growth medium. Cell suspensions were shaken for 30 min at 37°C and plated on collagen-coated 6-well plates. For isolation of adult keratinocytes, 4–8-wk-old mice were used. Tail skin was sterilized by incubation for 5 min in iodine solution, PBS, and 70% EtOH and floated, dermal side down, on 0.25% trypsin (without EDTA; Gibco) for 1.5 h at 37°C, 5% CO_2. Subsequently, epidermis was separated from the dermis, minced, and gently agitated for 30 min at 37°C in keratinocyte growth medium. After straining through a 70-µm filter, cell suspensions were centrifuged (850 g, 5 min, 22°C) and cultured as keratinocytes isolated from newborn mice.

Colony-forming assays
For colony-forming assays, 2,000 primary keratinocytes (passage 0–3) were plated in triplicates in a 6-well plate and cultured for 3 wk in the presence of fibroblasts. Cells were fixed with 1% PFA for 15 min and subsequently stained for 1 h with 0.05% crystal violet in PBS. Digital images were analyzed for colony size and number using ImageJ (National Institutes of Health).

BrdU label retaining experiment
10-d-old mice were injected with 50 mg/kg bodyweight BrdU every 24 h for 3 injections. After a 15-, 40-, or 70-d chase period the mice were sacrificed and dorsal skin (day 15) and tail skin whole-mounts (day 40 and day 70) were isolated for immunohistochemical staining and analysis (Braun et al., 2003).

Division axis orientation determination
The axis of divisions in E16.5 embryos was determined in anaphase/telophase cells using survivin staining and K14 as described by Williams et al. (2011). The angle of division was determined by measuring the angle of the plane transecting two daughter cells relative to the plane of the basement membrane. The different divisions were then categorized as described with asymmetric divisions having an angle of 60–90 degrees, random 30–60 degrees, and symmetric 0 and 30 degrees (Lechler and Fuchs, 2005). For HFs, survivin was costained with K15 to label the bulge region. The division axis was measured with respect to the long axis of hair follicle growth cells. The angles of divisions were quantified with total division number set to 100% and angle orientation was plotted with Oriana 4 (Kovach Computing Services). Division angles within 0–30 degrees parallel to the long hair follicle axis were scored as symmetric, whereas divisions perpendicular (within 60–90 degrees) to the axis were scored as asymmetric. Total number of asymmetric and symmetric divisions was set to 100% within the whole HF or within specific regions, with K15 identifying the bulge HF, and the JZ as the area identified above the K15-positive area. For P0 and P6 we only quantified the whole HF, as the bulge region is not clearly defined at this time point.

Quantitative RT-PCR
RNA was extracted from isolated epidermis or from FACS-sorted keratinocytes using the RNeasy Minikit (QIAGEN) according to the manufacturer's instructions. cDNA was prepared using at least 500 ng of RNA by a reverse-transcription reaction using Quantitect Reverse transcription (QIAGEN) according to the manufacturer's instructions. cDNA quality was checked by GAPDH and actin PCR. Taqman assays were purchased from Applied Biosystems. To analyze gene expression of target genes, cDNA was amplified using TaqMan Universal PCR Master Mix. Quantitative PCR was performed on a sequence detector (ABI-PRISM 7700; Applied Biosystems). Assays were linear over four orders of magnitude. The expression levels of the genes were shown as percentage of GAPDH expression using DCt for

calculation. For the calculation of the t test, DDCt values were calculated using the mean Ctr value.

FACS analysis/sorting from adult mice
Primary adult keratinocytes were isolated as described previously (Blanpain et al., 2004). After filtering through a 70-µm and 40-µm cell strainer, single cell suspensions were incubated in 5% FCS/PBS with antibodies for 45 min at 4°C. Cell viability was assessed by 7AAD (BD) labeling. Subsequent analysis was performed using a FACSCanto II cytometer (BD) equipped with FACS-Diva Software (BD). Cell sorting for RNA isolation was performed using a FACSVantage SE system (BD).

Statistical analysis
Statistical significance was performed as unpaired Student's t test using Microsoft Excel and Prism software (GraphPad Software). Error bars indicate the mean ± SD of the mean. P values: *, $P < 0.05$; **, $P < 0.005$; ***, $P < 0.0005$.

Online supplemental material
Fig. S1 shows efficient epidermis-specific deletion of aPKCλ in aPKCλ[epi−/−] mice. Fig. S2 shows altered morphology of the epidermis and appendages upon loss of aPKCλ. Fig. S3 shows altered hair follicle differentiation in aPKCλ^{−/−} mice. Fig. S4 shows loss of bulge stem cell markers over time. Fig. S5 shows stem and progenitor cell changes upon loss of aPKCλ. Table S1 and S2 show overview of antibodies and microscope contribution, respectively. Online supplemental material is available at http://www.jcb.org/cgi/content/full/jcb.201307001/DC1.

References

Bandyopadhyay, G., M.L. Standaert, M.P. Sajan, Y. Kanoh, A. Miura, U. Braun, F. Kruse, M. Leitges, and R.V. Farese. 2004. Protein kinase C-lambda knockout in embryonic stem cells and adipocytes impairs insulin-stimulated glucose transport. *Mol. Endocrinol.* 18:373–383. http://dx.doi.org/10.1210/me.2003-0087

Barker, N., J.H. van Es, J. Kuipers, P. Kujala, M. van den Born, M. Cozijnsen, A. Haegebarth, J. Korving, H. Begthel, P.J. Peters, and H. Clevers. 2007. Identification of stem cells in small intestine and colon by marker gene Lgr5. *Nature.* 449:1003–1007. http://dx.doi.org/10.1038/nature06196

Barrandon, Y., and H. Green. 1987. Three clonal types of keratinocyte with different capacities for multiplication. *Proc. Natl. Acad. Sci. USA.* 84:2302–2306. http://dx.doi.org/10.1073/pnas.84.8.2302

Baye, L.M., and B.A. Link. 2007. Interkinetic nuclear migration and the selection of neurogenic cell divisions during vertebrate retinogenesis. *J. Neurosci.* 27:10143–10152. http://dx.doi.org/10.1523/JNEUROSCI.2754-07.2007

Blanpain, C., and E. Fuchs. 2009. Epidermal homeostasis: a balancing act of stem cells in the skin. *Nat. Rev. Mol. Cell Biol.* 10:207–217. http://dx.doi.org/10.1038/nrm2636

Blanpain, C., W.E. Lowry, A. Geoghegan, L. Polak, and E. Fuchs. 2004. Self-renewal, multipotency, and the existence of two cell populations within an epithelial stem cell niche. *Cell.* 118:635–648. http://dx.doi.org/10.1016/j.cell.2004.08.012

Braun, K.M., C. Niemann, U.B. Jensen, J.P. Sundberg, V. Silva-Vargas, and F.M. Watt. 2003. Manipulation of stem cell proliferation and lineage commitment: visualisation of label-retaining cells in wholemounts of mouse epidermis. *Development*. 130:5241–5255. http://dx.doi.org/10.1242/dev.00703

Castilho, R.M., C.H. Squarize, L.A. Chodosh, B.O. Williams, and J.S. Gutkind. 2009. mTOR mediates Wnt-induced epidermal stem cell exhaustion and aging. *Cell Stem Cell*. 5:279–289. http://dx.doi.org/10.1016/j.stem.2009.06.017

Clayton, E., D.P. Doupé, A.M. Klein, D.J. Winton, B.D. Simons, and P.H. Jones. 2007. A single type of progenitor cell maintains normal human epidermis. *Nature*. 446:185–189. http://dx.doi.org/10.1038/nature05574

Dard, N., T. Le, B. Maro, and S. Louvet-Vallée. 2009. Inactivation of aPKClambda reveals a context dependent allocation of cell lineages in preimplantation mouse embryos. *PLoS ONE*. 4:e7117. http://dx.doi.org/10.1371/journal.pone.0007117

de Navascués, J., C.N. Perdigoto, Y. Bian, M.H. Schneider, A.J. Bardin, A. Martínez-Arias, and B.D. Simons. 2012. *Drosophila* midgut homeostasis involves neutral competition between symmetrically dividing intestinal stem cells. *EMBO J.* 31:2473–2485. http://dx.doi.org/10.1038/emboj.2012.106

Durgan, J., N. Kaji, D. Jin, and A. Hall. 2011. Par6B and atypical PKC regulate mitotic spindle orientation during epithelial morphogenesis. *J. Biol. Chem.* 286:12461–12474. http://dx.doi.org/10.1074/jbc.M110.174235

Encinas, J.M., T.V. Michurina, N. Peunova, J.H. Park, J. Tordo, D.A. Peterson, G. Fishell, A. Koulakov, and G. Enikolopov. 2011. Division-coupled astrocytic differentiation and age-related depletion of neural stem cells in the adult hippocampus. *Cell Stem Cell*. 8:566–579. http://dx.doi.org/10.1016/j.stem.2011.03.010

Farese, R.V., M.P. Sajan, H. Yang, P. Li, S. Mastorides, W.R. Gower Jr., S. Nimal, C.S. Choi, S. Kim, G.I. Shulman, et al. 2007. Muscle-specific knockout of PKC-lambda impairs glucose transport and induces metabolic and diabetic syndromes. *J. Clin. Invest.* 117:2289–2301. http://dx.doi.org/10.1172/JCI31408

Fields, A.P., L.A. Frederick, and R.P. Regala. 2007. Targeting the oncogenic protein kinase Ciota signalling pathway for the treatment of cancer. *Biochem. Soc. Trans.* 35:996–1000. http://dx.doi.org/10.1042/BST0350996

Goulas, S., R. Conder, and J.A. Knoblich. 2012. The Par complex and integrins direct asymmetric cell division in adult intestinal stem cells. *Cell Stem Cell*. 11:529–540. http://dx.doi.org/10.1016/j.stem.2012.06.017

Hafner, M., J. Wenk, A. Nenci, M. Pasparakis, K. Scharffetter-Kochanek, N. Smyth, T. Peters, D. Kess, O. Holtkötter, P. Shephard, et al. 2004. Keratin 14 Cre transgenic mice authenticate keratin 14 as an oocyte-expressed protein. *Genesis*. 38:176–181. http://dx.doi.org/10.1002/gene.20016

Hao, Y., Q. Du, X. Chen, Z. Zheng, J.L. Balsbaugh, S. Maitra, J. Shabanowitz, D.F. Hunt, and I.G. Macara. 2010. Par3 controls epithelial spindle orientation by aPKC-mediated phosphorylation of apical Pins. *Curr. Biol.* 20:1809–1818. http://dx.doi.org/10.1016/j.cub.2010.09.032

Helfrich, I., A. Schmitz, P. Zigrino, C. Michels, I. Haase, A. le Bivic, M. Leitges, and C.M. Niessen. 2007. Role of aPKC isoforms and their binding partners Par3 and Par6 in epidermal barrier formation. *J. Invest. Dermatol.* 127:782–791. http://dx.doi.org/10.1038/sj.jid.5700621

Horsley, V., A.O. Aliprantis, L. Polak, L.H. Glimcher, and E. Fuchs. 2008. NFATc1 balances quiescence and proliferation of skin stem cells. *Cell*. 132:299–310. http://dx.doi.org/10.1016/j.cell.2007.11.047

Hsu, Y.C., H.A. Pasolli, and E. Fuchs. 2011. Dynamics between stem cells, niche, and progeny in the hair follicle. *Cell*. 144:92–105. http://dx.doi.org/10.1016/j.cell.2010.11.049

Iden, S., W.E. van Riel, R. Schäfer, J.Y. Song, T. Hirose, S. Ohno, and J.G. Collard. 2012. Tumor type-dependent function of the par3 polarity protein in skin tumorigenesis. *Cancer Cell*. 22:389–403. http://dx.doi.org/10.1016/j.ccr.2012.08.004

Imai, F., S. Hirai, K. Akimoto, H. Koyama, T. Miyata, M. Ogawa, S. Noguchi, T. Sasaoka, T. Noda, and S. Ohno. 2006. Inactivation of aPKClambda results in the loss of adherens junctions in neuroepithelial cells without affecting neurogenesis in mouse neocortex. *Development*. 133:1735–1744. http://dx.doi.org/10.1242/dev.02330

Jaks, V., N. Barker, M. Kasper, J.H. van Es, H.J. Snippert, H. Clevers, and R. Toftgård. 2008. Lgr5 marks cycling, yet long-lived, hair follicle stem cells. *Nat. Genet.* 40:1291–1299. http://dx.doi.org/10.1038/ng.239

Jaks, V., M. Kasper, and R. Toftgård. 2010. The hair follicle-a stem cell zoo. *Exp. Cell Res.* 316:1422–1428. http://dx.doi.org/10.1016/j.yexcr.2010.03.014

Jensen, K.B., C.A. Collins, E. Nascimento, D.W. Tan, M. Frye, S. Itami, and F.M. Watt. 2009. Lrig1 expression defines a distinct multipotent stem cell population in mammalian epidermis. *Cell Stem Cell*. 4:427–439. http://dx.doi.org/10.1016/j.stem.2009.04.014

Knoblich, J.A. 2010. Asymmetric cell division: recent developments and their implications for tumour biology. *Nat. Rev. Mol. Cell Biol.* 11:849–860. http://dx.doi.org/10.1038/nrm3010

Kobielak, K., N. Stokes, J. de la Cruz, L. Polak, and E. Fuchs. 2007. Loss of a quiescent niche but not follicle stem cells in the absence of bone morphogenetic protein signaling. *Proc. Natl. Acad. Sci. USA*. 104:10063–10068. http://dx.doi.org/10.1073/pnas.0703004104

Kovac, J., H. Oster, and M. Leitges. 2007. Expression of the atypical protein kinase C (aPKC) isoforms iota/lambda and zeta during mouse embryogenesis. *Gene Expr. Patterns*. 7:187–196. http://dx.doi.org/10.1016/j.modgep.2006.07.002

Langbein, L., H. Spring, M.A. Rogers, S. Praetzel, and J. Schweizer. 2004. Hair keratins and hair follicle-specific epithelial keratins. *Methods Cell Biol.* 78:413–451. http://dx.doi.org/10.1016/S0091-679X(04)78015-2

Lechler, T., and E. Fuchs. 2005. Asymmetric cell divisions promote stratification and differentiation of mammalian skin. *Nature*. 437:275–280. http://dx.doi.org/10.1038/nature03922

Lee, C.Y., K.J. Robinson, and C.Q. Doe. 2006. Lgl, Pins and aPKC regulate neuroblast self-renewal versus differentiation. *Nature*. 439:594–598. http://dx.doi.org/10.1038/nature04299

Leitges, M., L. Sanz, P. Martin, A. Duran, U. Braun, J.F. García, F. Camacho, M.T. Diaz-Meco, P.D. Rennert, and J. Moscat. 2001. Targeted disruption of the zetaPKC gene results in the impairment of the NF-kappaB pathway. *Mol. Cell.* 8:771–780. http://dx.doi.org/10.1016/S1097-2765(01)00361-6

Mascré, G., S. Dekoninck, B. Drogat, K.K. Youssef, S. Brohée, P.A. Sotiropoulou, B.D. Simons, and C. Blanpain. 2012. Distinct contribution of stem and progenitor cells to epidermal maintenance. *Nature*. 489:257–262. http://dx.doi.org/10.1038/nature11393

Miyata, T., D. Kawaguchi, A. Kawaguchi, and Y. Gotoh. 2010. Mechanisms that regulate the number of neurons during mouse neocortical development. *Curr. Opin. Neurobiol.* 20:22–28. http://dx.doi.org/10.1016/j.conb.2010.01.001

Miyazaki, M., W.C. Man, and J.M. Ntambi. 2001. Targeted disruption of stearoyl-CoA desaturase1 gene in mice causes atrophy of sebaceous and meibomian glands and depletion of wax esters in the eyelid. *J. Nutr.* 131:2260–2268.

Morris, R.J., and C.S. Potten. 1994. Slowly cycling (label-retaining) epidermal cells behave like clonogenic stem cells in vitro. *Cell Prolif.* 27:279–289. http://dx.doi.org/10.1111/j.1365-2184.1994.tb01425.x

Morris, R.J., Y. Liu, L. Marles, Z. Yang, C. Trempus, S. Li, J.S. Lin, J.A. Sawicki, and G. Cotsarelis. 2004. Capturing and profiling adult hair follicle stem cells. *Nat. Biotechnol.* 22:411–417. http://dx.doi.org/10.1038/nbt950

Murray, N.R., J. Weems, U. Braun, M. Leitges, and A.P. Fields. 2009. Protein kinase C betaII and PKCiota/lambda: collaborating partners in colon cancer promotion and progression. *Cancer Res.* 69:656–662. http://dx.doi.org/10.1158/0008-5472.CAN-08-3001

Nijhof, J.G., K.M. Braun, A. Giangreco, C. van Pelt, H. Kawamoto, R.L. Boyd, R. Willemze, L.H. Mullenders, F.M. Watt, F.R. de Gruijl, and W. van Ewijk. 2006. The cell-surface marker MTS24 identifies a novel population of follicular keratinocytes with characteristics of progenitor cells. *Development*. 133:3027–3037. http://dx.doi.org/10.1242/dev.02443

Petersson, M., H. Brylka, A. Kraus, S. John, G. Rappl, P. Schettina, and C. Niemann. 2011. TCF/Lef1 activity controls establishment of diverse stem and progenitor cell compartments in mouse epidermis. *EMBO J.* 30:3004–3018. http://dx.doi.org/10.1038/emboj.2011.199

Poulson, N.D., and T. Lechler. 2010. Robust control of mitotic spindle orientation in the developing epidermis. *J. Cell Biol.* 191:915–922. http://dx.doi.org/10.1083/jcb.201008001

Poulson, N.D., and T. Lechler. 2012. Asymmetric cell divisions in the epidermis. *Int Rev Cell Mol Biol.* 295:199–232. http://dx.doi.org/10.1016/B978-0-12-394306-4.00012-5

Quyn, A.J., P.L. Appleton, F.A. Carey, R.J. Steele, N. Barker, H. Clevers, R.A. Ridgway, O.J. Sansom, and I.S. Näthke. 2010. Spindle orientation bias in gut epithelial stem cell compartments is lost in precancerous tissue. *Cell Stem Cell*. 6:175–181. http://dx.doi.org/10.1016/j.stem.2009.12.007

Regala, R.P., R.K. Davis, A. Kunz, A. Khoor, M. Leitges, and A.P. Fields. 2009. Atypical protein kinase Ciota is required for bronchioalveolar stem cell expansion and lung tumorigenesis. *Cancer Res.* 69:7603–7611. http://dx.doi.org/10.1158/0008-5472.CAN-09-2066

Rolls, M.M., R. Albertson, H.P. Shih, C.Y. Lee, and C.Q. Doe. 2003. *Drosophila* aPKC regulates cell polarity and cell proliferation in neuroblasts and epithelia. *J. Cell Biol.* 163:1089–1098. http://dx.doi.org/10.1083/jcb.200306079

Sabherwal, N., A. Tsutsui, S. Hodge, J. Wei, A.D. Chalmers, and N. Papalopulu. 2009. The apicobasal polarity kinase aPKC functions as a nuclear determinant and regulates cell proliferation and fate during *Xenopus* primary neurogenesis. *Development*. 136:2767–2777. http://dx.doi.org/10.1242/dev.034454

Schweizer, J., L. Langbein, M.A. Rogers, and H. Winter. 2007. Hair follicle-specific keratins and their diseases. *Exp. Cell Res.* 313:2010–2020. http://dx.doi.org/10.1016/j.yexcr.2007.02.032

Sengupta, A., A. Duran, E. Ishikawa, M.C. Florian, S.K. Dunn, A.M. Ficker, M. Leitges, H. Geiger, M. Diaz-Meco, J. Moscat, and J.A. Cancelas. 2011. Atypical protein kinase C (aPKCzeta and aPKClambda) is dispensable for mammalian hematopoietic stem cell activity and blood formation. *Proc. Natl. Acad. Sci. USA*. 108:9957–9962. http://dx.doi.org/10.1073/pnas.1103132108

Smart, I.H. 1970. Variation in the plane of cell cleavage during the process of stratification in the mouse epidermis. *Br. J. Dermatol.* 82:276–282. http://dx.doi.org/10.1111/j.1365-2133.1970.tb12437.x

Snippert, H.J., L.G. van der Flier, T. Sato, J.H. van Es, M. van den Born, C. Kroon-Veenboer, N. Barker, A.M. Klein, J. van Rheenen, B.D. Simons, and H. Clevers. 2010. Intestinal crypt homeostasis results from neutral competition between symmetrically dividing Lgr5 stem cells. *Cell*. 143:134–144. http://dx.doi.org/10.1016/j.cell.2010.09.016

Soloff, R.S., C. Katayama, M.Y. Lin, J.R. Feramisco, and S.M. Hedrick. 2004. Targeted deletion of protein kinase C lambda reveals a distribution of functions between the two atypical protein kinase C isoforms. *J. Immunol.* 173:3250–3260.

Soriano, P. 1999. Generalized lacZ expression with the ROSA26 Cre reporter strain. *Nat. Genet.* 21:70–71. http://dx.doi.org/10.1038/5007

St Johnston, D., and J. Ahringer. 2010. Cell polarity in eggs and epithelia: parallels and diversity. *Cell*. 141:757–774. http://dx.doi.org/10.1016/j.cell.2010.05.011

Tanimura, S., Y. Tadokoro, K. Inomata, N.T. Binh, W. Nishie, S. Yamazaki, H. Nakauchi, Y. Tanaka, J.R. McMillan, D. Sawamura, et al. 2011. Hair follicle stem cells provide a functional niche for melanocyte stem cells. *Cell Stem Cell*. 8:177–187. http://dx.doi.org/10.1016/j.stem.2010.11.029

Tunggal, J.A., I. Helfrich, A. Schmitz, H. Schwarz, D. Günzel, M. Fromm, R. Kemler, T. Krieg, and C.M. Niessen. 2005. E-cadherin is essential for in vivo epidermal barrier function by regulating tight junctions. *EMBO J.* 24:1146–1156. http://dx.doi.org/10.1038/sj.emboj.7600605

Watt, F.M., and K.B. Jensen. 2009. Epidermal stem cell diversity and quiescence. *EMBO Mol Med*. 1:260–267. http://dx.doi.org/10.1002/emmm.200900033

Williams, S.E., S. Beronja, H.A. Pasolli, and E. Fuchs. 2011. Asymmetric cell divisions promote Notch-dependent epidermal differentiation. *Nature*. 470:353–358. http://dx.doi.org/10.1038/nature09793

Yang, L., L. Wang, and X. Yang. 2009. Disruption of Smad4 in mouse epidermis leads to depletion of follicle stem cells. *Mol. Biol. Cell*. 20:882–890. http://dx.doi.org/10.1091/mbc.E08-07-0731

Zhang, J., X.C. He, W.G. Tong, T. Johnson, L.M. Wiedemann, Y. Mishina, J.Q. Feng, and L. Li. 2006. Bone morphogenetic protein signaling inhibits hair follicle anagen induction by restricting epithelial stem/progenitor cell activation and expansion. *Stem Cells*. 24:2826–2839. http://dx.doi.org/10.1634/stemcells.2005-0544

Zhang, Y.V., J. Cheong, N. Ciapurin, D.J. McDermitt, and T. Tumbar. 2009. Distinct self-renewal and differentiation phases in the niche of infrequently dividing hair follicle stem cells. *Cell Stem Cell*. 5:267–278. http://dx.doi.org/10.1016/j.stem.2009.06.004